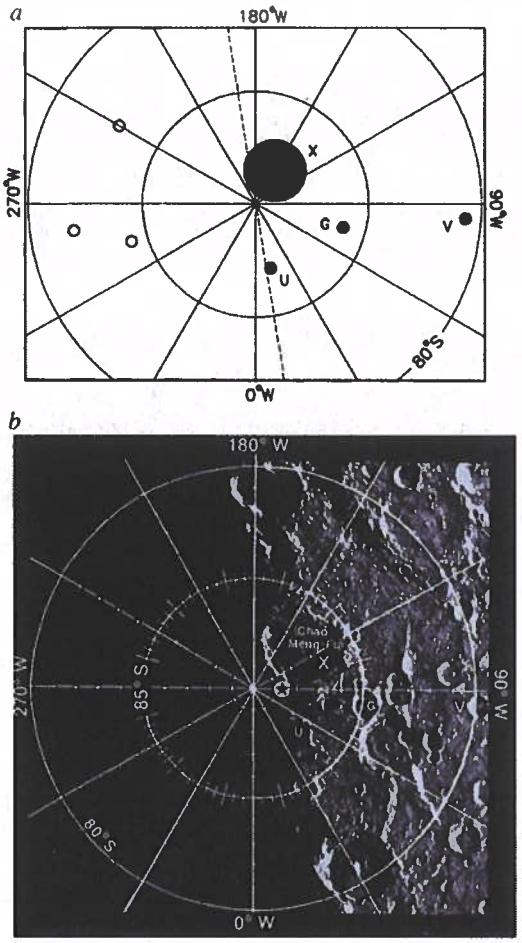

FIG. 3 Locating maps for south polar radar features. *a*, Locations of the letter-labelled features (filled circles) as well as some unlabelled features in the unphotographed hemisphere (open circles). The dashed line shows the location of the Mariner-10 terminator, the unphotographed hemisphere being to the left. *b*, Mariner-10 image of the south pole. There may be small discrepancies between the grid in *b* and the NASA/USGS grid due to distortions in the Mariner-10 image mosaics; there may therefore be differences between the crater positions in *b* and the crater coordinates listed in Table 1. Our estimate of the true south pole position is shown in *b* (star).

values of $\hat{\sigma}_u$ suggest that all of the identified source craters have enough shaded, radar-visible area to account for the high cross-sections. This seems to be the case even for features with latitudes as low as 80–81° (features S, T, V, W). However, permanent shadowing alone may not guarantee temperatures low enough to sustain ice[3,4], and additional theoretical work should be done to evaluate the plausibility of ice existing at these lower latitudes. Finally, Table 1 shows that the radar polarization of the features tends to be 'inverted' ($\mu_c > 1$); for the strongest of the features the measured inversion is statistically significant. Such polarization inversion is consistent with the X-band radar results for Mercury's north polar anomaly[1] and is reminiscent of the anomalous radar polarization of the icy galilean satellites[10] and Mars' southern icecap[11].

Our new images prove the connection between the radar anomalies and polar craters, and provide strong support for the notion that the radar-bright material is concentrated in permanently shaded crater floors. The most plausible model still seems to be one in which shaded crater floors act as cold traps for water ice, thick deposits of which provide a low-loss medium for enhanced volume backscatter of radio waves. Conclusive proof of the existence of polar ice will require spacecraft missions equipped with ultraviolet or neutron spectrometers and, possibly, sampling penetrators. The next mission to Mercury could, at the very least, provide the photoimaging necessary to (1) corroborate the cartographic grid refinements proposed here, and (2) identify source craters for those radar-bright spots which are presently located in unphotographed terrain. □

Received 22 February; accepted 5 April 1994.

1. Slade, M. A., Butler, B. J. & Muhleman, D. O. *Science* **258**, 635–640 (1992).
2. Harmon, J. K. & Slade, M. A. *Science* **258**, 640–643 (1992).
3. Paige, D. A., Wood, S. E. & Vasavada, A. R. *Science* **258**, 643–646 (1992).
4. Ingersoll, A. P., Svitek, T. & Murray, B. C. *Icarus* **100**, 40–47 (1992).
5. Butler, B. J., Muhleman, D. O. & Slade, M. A. *J. geophys. Res.* **98**, 15003–15023 (1993).
6. Davies, M. E., Dwornik, S. E., Gault, D. E. & Strom, R. G. *Atlas of Mercury* (NASA, Washington DC, 1978).
7. *Shaded Relief Map of Mercury* (USGS Map I-1149, US Geological Surv., Reston, Virginia, 1979).
8. Grolier, M. J. & Boyce, J. M. *Geologic Map of the Borealis Region of Mercury* (USGS Map I-1660, US Geological Surv., Reston, Virginia, 1984).
9. Strom, R. G., Malin, M. C. & Leake, M. A. *Geologic Map of the Bach Region of Mercury* (USGS Map I-2015, US Geological Surv., Reston, Virginia, 1990).
10. Ostro, S. J. *et al. J. geophys. Res.* **97**, 18227–18244 (1992).
11. Muhleman, D. O., Butler, B. J., Grossman, A. W. & Slade, M. A. *Science* **253**, 1508–1513 (1991).
12. Harmon, J. K., Slade, M. A. & Hudson, R. S. *Icarus* **98**, 240–253 (1992).
13. Davies, M. E. & Batson, R. M. *J. geophys. Res.* **80**, 2417–2430 (1975).

ACKNOWLEDGEMENTS. We thank R. Thomas, A. Venkataraman and P. Perillat for their assistance with computing. Ephemerides for the radar observations were supplied by the Center for Astrophysics. M.J.D. and J.M.J. were supported by the Arecibo summer student programme under a grant from the REU program of the US NSF. Part of this work was carried out under contract with NASA. The National Astronomy and Ionosphere Center (Arecibo Observatory) is operated by Cornell University under a cooperative agreement with the US NSF and with support from NASA.

Experimental observation of self-replicating spots in a reaction–diffusion system

Kyoung-Jin Lee*, William D. McCormick*, John E. Pearson† & Harry L. Swinney*

* Center for Nonlinear Dynamics and the Department of Physics, The University of Texas, Austin, Texas 78712, USA
† Center for Nonlinear Studies, Los Alamos National Laboratory, Los Alamos, New Mexico 87545, USA

In his classic 1952 paper, Turing[1] suggested a possible connection between patterns in biological systems and patterns that could form spontaneously in chemical reaction–diffusion systems. Turing's analysis stimulated considerable theoretical research on mathematical models of pattern formation, but Turing-type patterns were not observed in controlled laboratory experiments until 1990[2,3]. Subsequently there has been a renewed interest in chemical pattern formation and in the relationship of chemical patterns to the remarkably similar patterns observed in diverse physical and biological systems[4]. Numerical simulations of a simple model chemical system have recently revealed spot patterns that undergo a continuous process of 'birth' through replication and 'death' through overcrowding[5]. Here we report the observation of a similar phenomenon in laboratory experiments on the ferrocyanide–iodate–sulphite reaction. Repeated growth and replication can be observed for a wide range of experimental parameters, and can be reproduced by a simple two-species model, suggesting that replicating spots may occur in many reaction–diffusion systems.

The laboratory chemical patterns form in a thin transparent gel (0.4 mm thick, 22 mm diameter) whose bottom surface is in contact with a well-stirred reservoir (3.0 ml volume) that is continuously refreshed with the reagents of the reaction[6]. Transitions are studied by changing the input ferrocyanide concentration with other parameters held fixed. In the parameter range studied, the concentrations in the reservoir are independent of time. Spatial variations of the chemical concentrations in the plane of the gel—that is, chemical patterns—are viewed with a video camera in reflected light in a band centred at 420 nm, where ferrocyanide absorbs strongly.

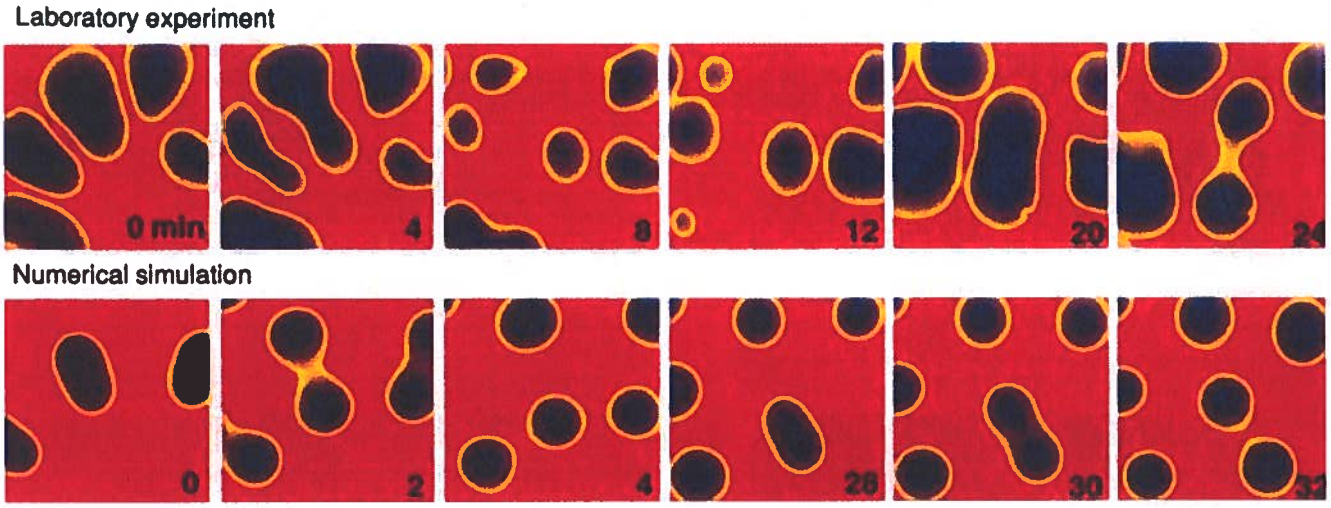

FIG. 1 The upper row of images shows the evolution of a chemical pattern observed in a laboratory experiment, and the lower row shows similar behaviour found in a numerical simulation of a reaction–diffusion model (see text). The behaviour illustrated here continues indefinitely, as long as the reactor conditions are maintained. In the experiment, blue (red) represents a state of high (low) pH, and the domain size is 7 mm × 7 mm. The concentrations of the reagents fed into the reservoir that is in contact with the gel reactor are (in mM): $[NaIO_3]=75.0$, $[Na_2SO_3]=89.0$, $[H_2SO_4]=3.6$, $[NaOH]=0.25$ and $[K_4Fe(CN)_6\cdot 3H_2O]=36.4$. The total input flow rate is 86.4 ml h^{-1}, and the reactor temperature is 30 °C. The dimensionless parameter values for the numerical simulation are $A=0.02$, $B=0.079$ and $D_U=2\times D_V=2.0\times 10^{-5}$; each panel shows a 150 × 150 pixel region from a domain of 512 × 512 pixels. The images from the simulation are coded red ($U=1$, $V=0$) and blue ($U=0.3$, $V=0.25$) and are labelled with dimensionless time/100.

Numerical simulations were conducted for a two-dimensional reaction–diffusion model system with the reaction $U+2V\rightarrow 3V$ coupled to a reservoir held at the fixed concentrations (U_0, V_0) (ref. 5):

$$\frac{\partial U}{\partial t}=D_U\nabla^2U-UV^2+A(U_0-U)$$

$$\frac{\partial V}{\partial t}=D_V\nabla^2V+UV^2+B(V_0-V)$$

where ($U_0=1$, $V_0=0$). The parameters A and B represent the strengths of the coupling of U and V to the reservoir, D_U and D_V are the diffusion coefficients, and t is time. In a homogeneous system our model exhibits oscillations and bistability, just as found in experiments and models for the well-studied Belousov–Zhabotinsky, chlorite–iodide–malonic acid, and ferrocyanide–iodate–sulphite[7] reactions. The differences in the pattern-forming behaviour of these systems stem in part from differences in the relative diffusion coefficients of different species in the reactions.

Numerical simulations of this reaction–diffusion model were performed in an attempt to find stationary lamellar patterns like those observed in an earlier experiment on the ferrocyanide–iodate–sulphite reactions[6]. The model yielded not only lamellar patterns but also self-replicating spots, as shown in Fig. 1, and other patterns[5]. A subsequent search for spots in the experiments

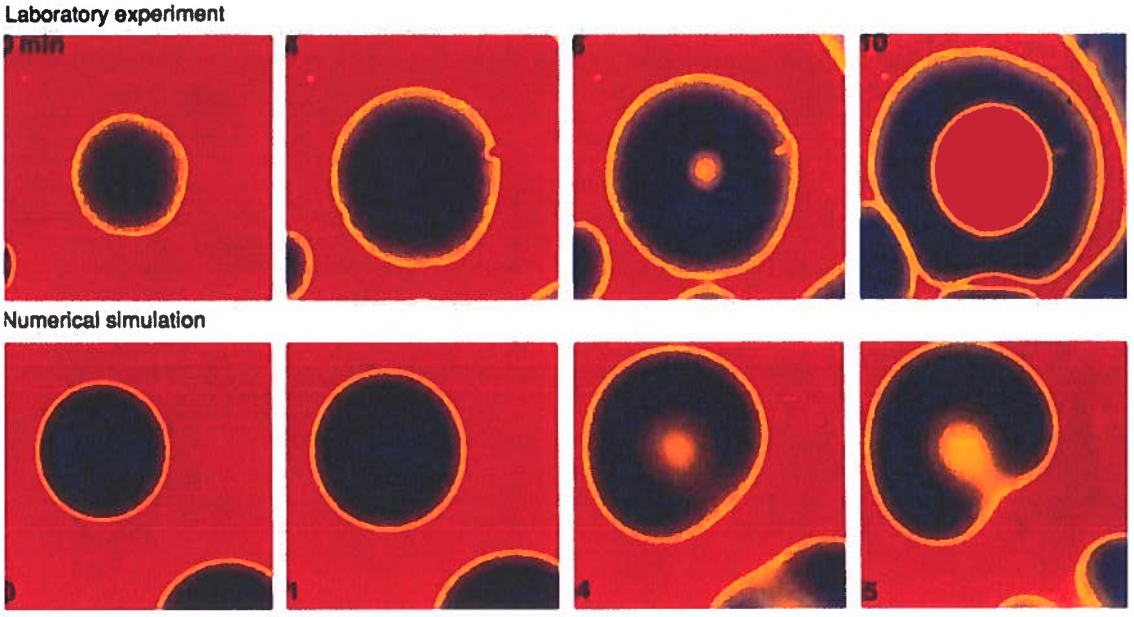

FIG. 2 Sequences showing the transition from a spot to an annulus in the experiments (upper row, 10 mm × 10 mm domain) and simulations (lower row, 120 × 120 pixel domain). The parameter values are the same as in Fig. 1.

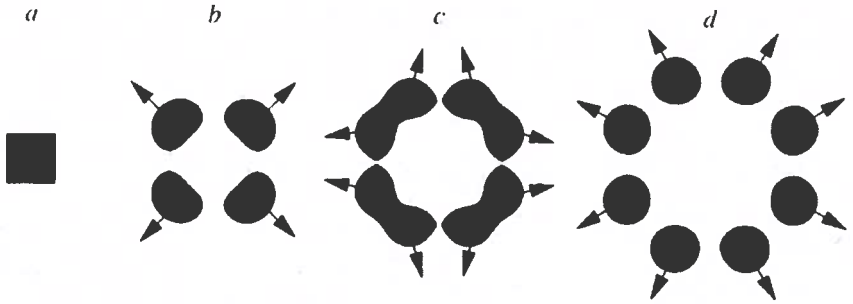

FIG. 3 Evolution of a square perturbation ($U=0.5$, $V=0.25$) of the initially homogeneous state ($U=1$, $V=0$). The initial square (*a*) is 50 × 50 pixels in a reaction domain of 512 × 512 pixels. *a*, *b*, *c* and *d*, Images corresponding to $t=0$, 4.2, 7.0 and 9.8 (dimensionless time/100), respectively (black, $U<0.44$).

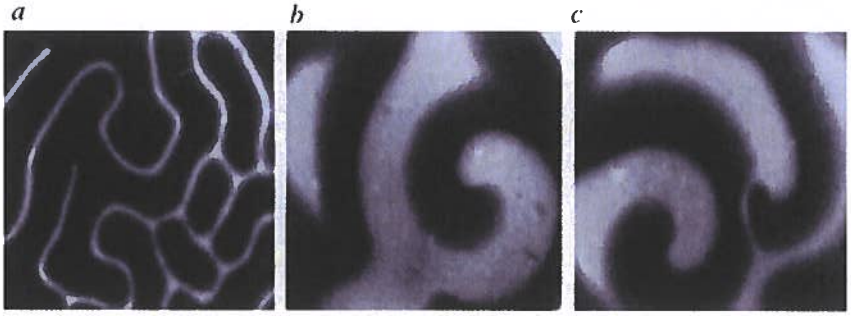

FIG. 4 Patterns formed at lower ferrocyanide concentrations than in Figs 1 and 2. *a*, Lamellar pattern; *b*, rotating spiral waves with wavefront annihilation; *c*, rotating spiral waves with wavefront repulsion. The high- and low-pH regions show as dark and light, respectively. The ferrocyanide concentrations in the feed are 14.2, 25.0 and 30.0 mM, respectively. Each frame is 18 mm × 18 mm.

produced not only spots but also annular patterns, as shown in Fig. 2. The annular patterns were then found in the model as well.

Spots do not form spontaneously from a uniform state in either the experiments or simulations. But once they have been initiated by a perturbation, the replicating spot patterns are self-sustaining. In the experiments, spots can be initiated by a perturbation using ultraviolet light or an inhomogeneity at the boundary.

Insight into the self-replicating behaviour can be gained from consideration of the evolution of spots in the model[8]. A spot, a region of high V and low U, is maintained by the diffusive flux of U (the more rapidly diffusing species) into the spot. Inside the spot, U is converted to V, while the spot loses V through diffusion into the reservoir and the spot's surroundings. Whether a spot grows or shrinks depends on the magnitude of the flux F of U through the spot's boundary. There is a critical flux of U, F_c, above (below) which the boundary moves toward the region of higher (lower) U.

The spot replication process is illustrated in Fig. 3, which shows the evolution of a square-shaped perturbation of the homogeneous state. The initial growth is largest in the corners of the square where the curvature is largest. The flux of U into the centre of the square is insufficient to maintain this region in the high-V state, and it collapses, leaving elongated spots at the corners of the square (Fig. 3*b*). These spots move outward along the diagonals because $F>F_c$ from the region outside the square while $F<F_c$ from inside. The decrease of U in the centre of a spot as it grows leads to a rapid decrease in V in the spot's centre. The spot then grows more rapidly in the direction orthogonal to the diagonals than along the diagonals. Hence the spot starts to pinch (Fig. 3*c*) and eventually divides into two daughter spots (Fig. 3*d*). This replication process happens repeatedly.

Spots repel each other when they approach very close because the region between them becomes depleted in U. If spots become overcrowded, many of them die. The flux of U into a surviving isolated spot is almost isotropic, and the spot expands until the flux of U is insufficient to maintain the spot centre in the high-V state. Then the centre collapses, leaving an annular ring, as shown in Fig. 2. These annular structures eventually break into pieces through interactions with neighbours.

We now describe the patterns observed for ferrocyanide concentrations lower and higher than the range in which spots form. At low ferrocyanide concentrations, domains of low pH spontaneously emerge from a uniform high-pH state. Each domain grows, and then shrinks to a thin stripe with a well-defined thickness. These stripes move and interact until the entire domain is filled with a stationary lamellar pattern, as shown in Fig. 4*a*. Although the pattern is irregular, there are well-defined length scales associated with the high- and low-pH regions. The lamellar pattern looks similar to those previously observed[6], but the previous patterns required a finite-amplitude perturbation for their initiation.

When the ferrocyanide concentration is increased, spiral waves form (Fig. 4*b*). As in the classic Belousov–Zhabotinsky reactions[9,10], these spiral waves annihilate upon collision, forming cusps (see the upper-right corner in Fig. 4*b*). The characteristic size of these spirals is much larger than the replicating spots.

When the ferrocyanide concentration is further increased in the direction that yields the replicating spots, the behaviour of two colliding fronts becomes quite different from that in excitable media: instead of annihilating on collision, fronts approach one another but remain separated by a sustained narrow zone of low pH; see Fig. 4*c*. Then one (or both) of the waves breaks and the broken ends become spiral tips, a process that leads to a large number of spiral tips. At yet higher ferrocyanide concentration, the new front interactions dominate, leading to many small wave segments, and eventually the system enters the replicating spot state illustrated in Fig. 1. For ferrocyanide concentration values beyond those of the replicating spot regime, the system goes into the homogeneous low-pH state. The transitions from Fig. 4*b* to *c* and from Fig. 4*c* to Fig. 1 are not sharp. In parameter ranges near each transition, both types of patterns can occur in different parts of the gel reactor.

The annihilation of colliding fronts is also found in the model, but for lower values of B than used in the simulations we have described. Smaller values of B sustain higher values of U between two approaching fronts, enough to maintain the propagation of fronts until they collide and annihilate.

In conclusion, spot replication and annuli are observed for a wide parameter range in the experiments on the ferrocyanide–iodate–sulphite reaction, and these observations are qualitatively described by a simple two-species model, as Figs 1 and 2 illustrate. The growth and interaction of spots and annuli lead to very complicated spatiotemporal patterns that continue to evolve indefinitely. Replicating spots, along with the previously

studied spirals[9,10], Turing patterns[2,3,11], and lamellae[6,12,13] can be expected to form in many reaction-diffusion systems maintained far from equilibrium. □

Received 19 January, accepted 29 March 1994.

1. Turing, A. M. *Phil. Trans. R. Soc.* **B327,** 37–72 (1952).
2. Castets, V., Dulos, E., Boissonade, J. & De Kepper, P. *Phys. Rev. Lett.* **64,** 2953–2965 (1990).
3. Ouyang, Q. & Swinney, H. L. *Nature* **352,** 610–612 (1991).
4. Cross, M. C. & Hohenberg, P. C. *Rev. mod. Phys.* **65,** 851–1112 (1993).
5. Pearson, J. E. *Science* **261,** 189–192 (1993).
6. Lee, K. J., McCormick, W. D., Ouyang, Q. & Swinney, H. L. *Science* **261,** 192–194 (1993).
7. Gáspár, V. & Showalter, K. *J. phys. Chem.* **94,** 4973–4979 (1990).
8. Reynolds, W. N., Pearson, J. E. & Ponce-Dawson, S. *Phys. Rev. Lett.* **72,** 2797–2800 (1994).
9. Zaikin, A. N. & Zhabotinskii, A. M. *Nature* **225,** 535–537 (1970).
10. Winfree, A. T. *Science* **175,** 634–636 (1972).
11. De Kepper, P., Perraud, J. J., Rudovics, B. & Dulos, E. *Int. J. Bifurcation Chaos* (submitted).
12. Petrich, D. M. & Goldstein, R. E. *Phys. Rev. Lett.* **72,** 1120–1123 (1994).
13. Hagberg, A. & Meron, E. *Phys. Rev. Lett.* **72,** 2494–2497 (1994).

ACKNOWLEDGEMENTS. We thank Q. Ouyang, S. Ponce-Dawson and W. Reynolds for discussions. This research is supported by the US Department of Energy Office of Basic Energy Sciences and the Robert A. Welch Foundation.

Chemical self-replication of palindromic duplex DNA

T. Li & K. C. Nicolaou*

Department of Chemistry, The Scripps Research Institute, 10666 North Torrey Pines Road, La Jolla, California 92037, USA and Department of Chemistry, University of California, San Diego, 9500 Gilman Drive, La Jolla, California 92093, USA

MOLECULAR replication, a fundamental process of life, has in recent years been the subject of laboratory investigations using simple chemical systems[1–10]. Whereas the work of Rebek's group[4,5] has focused on molecular architectures not known in living systems, self-replicating and template-based self-assembling systems based on nucleotides[6–8] are regarded as potential models for exploring the evolution of replicating systems on the early Earth. Previous replicating oligonucleotides have been of the single-stranded, self-complementary type: small oligonucleotide fragments are assembled on a pre-existing template and linked to form an exact copy of the template. This process cannot easily be reiterated, however, because of the strong binding of the newly formed strand to the original template. Furthermore, DNA replication in living systems operates by complementarity rather than self-complementarity—each newly assembled strand is complementary to, rather than identical to, its template—and the replication process starts and finishes with double helices. Here we report the self-replication of palindromic (symmetrical) duplex DNA-like oligonucleotides, 24 monomers long, in the absence of enzymes by means of a cycle that transfers information from template to copy and is potentially capable of extension to include non-symmetrical sequences, selection and mutation. Replication proceeds by a chemical process involving the formation of an intermediate triplex structure, and is sequence-selective in the sense that mismatches impair its efficiency. These results indicate that DNA-like double-helical molecules can replicate without assistance from proteins, a finding that may be relevant both to the appearance of replicating systems on the early Earth and to the development of new approaches to DNA amplification.

Figure 1*a* depicts the self-replication cycle that we have designed, which is based on the well-known principles of triple-strand[10,11] (Watson–Crick–Hoogsteen) and double-strand (Watson–Crick) DNA formation. It was anticipated that the relatively weaker Hoogsteen binding involved in triple helices would allow release of the newly generated strand from a double helical

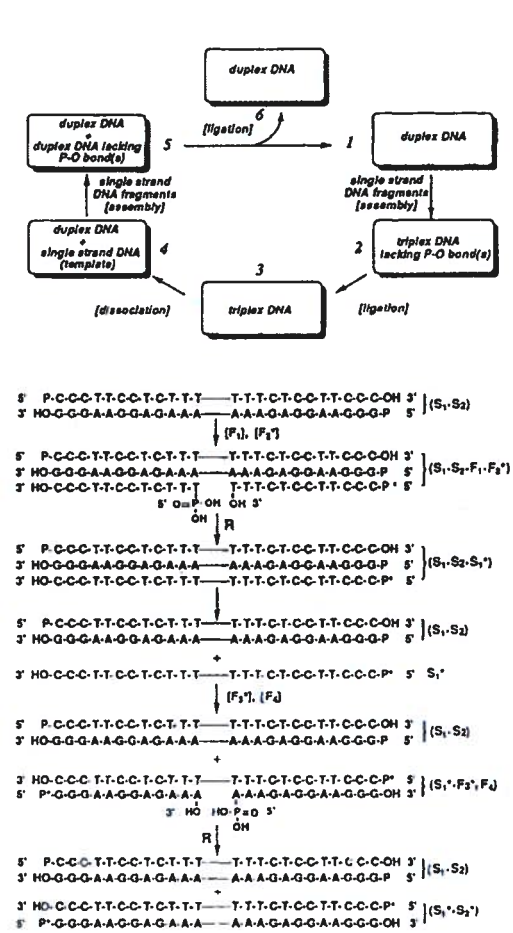

FIG. 1 *a*, General schematic representation of chemical self-replication of a palindromic duplex DNA cycle by triple- and double-helix formation. *b*, Replication of duplex DNA as a result of sequential triple- and double-helix formation. Sequences of oligodeoxyribonucleotides used: F_1 is 5′ P-TTTCTCCTTCCC-OH 3′; F_2 is 5′ P*-CCCTTCCTCTTT-OH 3′; F_3 is 5′ P*-GGGAAGGAGAAA-OH 3′; F_4 is 5′ P-AAAGAGGAAGGG-OH 3′. The asterisk designates radiolabelled (^{32}P) 5′ phosphorus (unlabelled: labelled ≈100). R is the reagent *N*-cyanoimidazole. Oligonucleotides were purchased from Operon Technologies. For details of experimental conditions, see text and legends to Figs 2–4.

template[12], thus ensuring, in combination with double-strand formation, continuous production of new copies. According to this scheme, duplex DNA serves, at an appropriately acidic pH, as a template to attract complementary single-strand DNA fragments, pre-organizing them along its major groove and orienting them in the right direction for ligation (1→2, Fig. 1*a*)[13]. A suitable chemical reagent then brings about P–O bond formation[13] thus forming a new strand, identical with one of the two strands of the original duplex (2→3). Raising the pH (pH driven) or adding an excess of oligonucleotides complementary to the newly formed strand drives the equilibrium away from the triplex structure, releasing the single strand (3→4), thus allowing it to serve as a template for duplex formation in the presence of complementary single-strand DNA fragments (4→5)[14–18]. Finally, a chemical reagent causing P–O bond formation[18] completes the cycle by generating a new strand identical to the second strand of the original DNA in an overall process that accomplishes replication of the original duplex (5→1, 6). This scheme, of course, requires symmetrical sequences, otherwise the product of the cycle is of the retro-sense. In the latter case (non-palindromic sequences) a second cycle and appropriate substrate fragments

* To whom correspondence should be addressed.